

# Construction of a Michelson Interferometer for Fourier Spectroscopy

Howard N. Rundle\*

(June 29, 1964)

The properties of the method employing a double beam interferometer for Fourier spectroscopy are briefly presented. A Michelson interferometer is described which is suitable for use in Fourier spectroscopy in the 1 to 10 micron region. The instrument can be used at any resolving power up to about  $10^5$ .

## 1. Introduction

Michelson [1,2]<sup>1</sup> showed the usefulness of the interferometer that bears his name. He showed that the intensity of the light measured at the output of his device is the Fourier transform of the incident optical spectra. Lord Rayleigh [3] showed how the observation of the visibility of the fringes could give the spectral profile of a symmetrical line. With the development of infrared detectors, Rubens and Wood [4] measured an "interferogram" and calculated a spectrum from this. The interferogram is the output measured from a Michelson interferometer.

Because of the availability of modern computers, this method has recently been revived [5,6, and 7]. Connes [8] has presented a detailed theory of the complete method. The following presents a brief outline of the properties of the method, and a description of an instrument with design criteria.

## 2. Properties of the Method

Figure 1 shows a schematic of a Michelson interferometer. Light from an extended source is collimated by lens  $L_1$ . The separating plate, S.P., has a reflectance and transmission of one-half and the reflected light from mirrors  $M_1$  and  $M_2$  is recombined by S.P., thereby forming circular fringes which are focused by lens  $L_2$  at the exit aperture. This aperture isolates the central fringe and a detector then detects the resultant intensity called the interferogram,  $I(\delta)$ , where  $\delta$  is the path difference  $2(d_2 - d_1)n$ ; and  $n$  is the index of refraction. The fringes of such a double beam interferometer are described by

$$F(\delta) = B \cos^2(\pi\sigma_0\delta) \\ = \frac{B}{2} [1 + \cos(2\pi\sigma_0\delta)] \quad (1)$$

where  $B$  is the intensity of the incident monochromatic radiation of wavenumber  $\sigma_0$ . If a spectrum

$B(\sigma)$  is incident on the interferometer, instead of a monochromatic spectrum, the interferogram is given by the sum of many such fringes or

$$I(\delta) = \int_0^\infty B(\sigma) \cos(2\pi\sigma\delta) d\sigma, \quad (2)$$

where the  $d-c$  term is dropped. That is,  $I(\delta)$  is the cosine transform of the incident spectra.

The interferogram,  $I(\delta)$ , is measured as a function of  $\delta$  and the spectrum  $B(\sigma)$  is given by

$$B(\sigma) = \int_0^\infty I(\delta) \cos 2\pi\sigma\delta d\delta. \quad (3)$$

Since it is physically possible to vary  $\delta$  from 0 to only  $\delta_M$ , one calculates

$$B'(\sigma) = \int_0^{\delta_M} I(\delta) \cos 2\pi\sigma\delta d\delta$$

which may be written as

$$B'(\sigma) = \int_0^\infty A(\delta) I(\delta) \cos 2\pi\sigma\delta d\delta \quad (4)$$

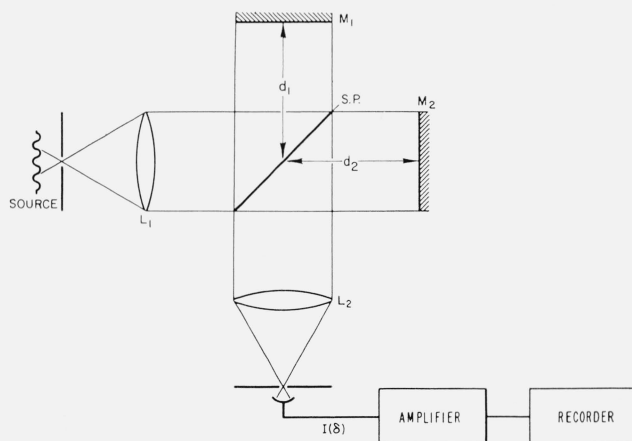


FIGURE 1. Michelson interferometer

\* Department of Physics, University of Saskatchewan, Saskatchewan, Canada.  
<sup>1</sup> Figures in brackets indicate the literature references at the end of this paper.

where

$$A(\delta) = \begin{cases} \alpha(\delta), & 0 \leq \delta \leq \delta_M \\ 0 & \text{elsewhere.} \end{cases}$$

$\alpha(\delta)$  can be taken as unity, but it is desirable to introduce a function for apodization.  $B'(\sigma)$  is an approximation to the actual incident spectrum  $B(\sigma)$  and can be calculated by an analog or digital method. The analog methods are useful for low resolving power (less than 1000) and at present digital methods must be used for higher resolving powers.

In an actual interferometer, flux is measured which implies that there are off-axis rays defining an angular field of solid angle  $\Omega$ . If these off-axis rays are considered [8],

$$B'(\sigma) = \frac{\Omega}{4\pi} \left[ \overline{B\left(\frac{\sigma}{1-\frac{\Omega}{4\pi}}\right)} + \overline{B\left(\frac{-\sigma}{1-\frac{\Omega}{4\pi}}\right)} \right] * T_c\{A(\delta)\} \quad (5)$$

where  $\overline{B}$  signifies the value obtained when  $B$  is smeared over a width of  $\frac{\sigma\Omega}{2\pi}$ ; i.e.,  $\overline{B}$  is the convolution of  $B$  with a slit or rectangle of unit height and width  $\frac{\sigma\Omega}{2\pi}$ . “\*” stands for the convolution product and  $T_c\{A(\delta)\}$  is the cosine transform of  $A(\delta)$  or

$$T_c\{A(\delta)\} = T_c[\alpha(\delta)] * \left\{ \delta_M \frac{\sin 2\pi\sigma\delta_M}{2\pi\sigma\delta_M} \right\}. \quad (6)$$

As  $B(\sigma)$  is smeared over a slit of width  $\frac{\Omega\sigma}{2\pi}$ , the resolution limit is  $\Delta\sigma = \frac{\sigma\Omega}{2\pi}$ ; or if  $R_t$  is the theoretical resolving power,

$$\Omega R_t = 2\pi. \quad (7)$$

From (6), the half width of  $\frac{\sin 2\pi\delta_M\sigma}{2\pi\delta_M\sigma}$  is  $\frac{1}{2\delta_M}$ . Therefore, if  $\alpha(\delta)=1$ , an optimum condition results if the resolution limit is also given by

$$\Delta\sigma = \frac{1}{2\delta_M}. \quad (8)$$

If  $\alpha(\delta) \neq 1$ , but is some function chosen to reduce the feet of  $\frac{\sin 2\pi\delta_M\sigma}{2\pi\delta_M\sigma}$ , i.e., apodization is performed [8], then the half width of the apodized function (6) is close to  $\frac{1}{\delta_M}$ , i.e.,

$$\Delta\sigma = \frac{1}{\delta_M}. \quad (9)$$

Equations (7) and (8) or (9) determine the maximum path difference and the output aperture diameter which are to be used. It should be noted that the theoretical resolving power  $R_t$  is reduced to about  $0.7R_t$  when (7) and (8) or (9) are considered.

In the above discussion, single-sided transforms have been used (i.e., integration from 0 to  $\infty$ ). In this method,  $I(\delta)$  is measured from 0 to  $\delta_M$ , and the assumption is made that if  $I(\delta)$  was measured from 0 to  $-\delta_M$ , the same result would be obtained. This is true only if the zero path difference occurs at the same place for all wave numbers. If this is not the case, one must know this phase shift (as it is called) and use it to find the zero path difference for each wave number. The same result can be accomplished by measuring  $I(\delta)$  from  $-\delta_M$  to 0 and to  $+\delta_M$ . Then double-sided transforms (i.e., integration from  $-\infty$  to  $+\infty$ ) are used. The same conclusions as stated in this section are obtained.

It is useful to point out some of the properties of the method. If  $B'(\sigma)$  is calculated from an interferogram that is digitized at every step  $h$  of  $\delta$ , one must assume that  $h \leq \frac{1}{2\sigma_M}$  where the incident spectra is nonzero in the region from 0 to  $\sigma_M$  only.

However, when noise is present,  $h$  must be smaller yet. In fact, if an R.C. time constant  $\tau$  is employed, then for the best signal to noise in  $B'(\sigma)$ ,  $h \approx \tau$  [8], where  $h$  is measured in seconds and the spectra is a function of frequency. In all the previous discussion, the path difference  $\delta$  can be replaced by time  $t$  and the wave number  $\sigma$  can be replaced by frequency  $\nu$ . When  $h = \tau$ , the spectral range in frequency units is from 0 to  $\frac{1}{2\pi\tau}$ .

A calculation of the signal-to-noise ratio obtained in the calculated spectra is complicated and the exact theory is not fully understood. However, the case when one is observing a monochromatic line only, has been presented [8]. In general, the signal-to-noise of the calculated spectra is

$$\left(\frac{S}{N}\right)_{\text{spectra}} \propto \beta \sqrt{\frac{T}{\xi}} \quad (10)$$

where  $T$  is the total time for one scan,  $\beta$  is the amplitude of the observed spectral element, and  $\xi$  is the noise amplitude.

In the case of a scanning instrument (i.e., spectrometer or Fabry-Perot)

$$\left(\frac{S}{N}\right)'_{\text{spectra}} \propto \beta \sqrt{\frac{T}{M\xi}} \quad (11)$$

where the time  $\frac{T}{M}$  is spent measuring each of the  $M$  spectral elements. Hence, if  $\xi$  is independent of the amount of incident radiation on the detector, as is the case for present day infrared detectors, the gain in the signal-to-noise which is realized with the interferometer is  $\sqrt{M}$  over that of a scanning instrument of the same light-gathering power, resolution, and detector. This gain is often referred to as “Fellgett’s Advantage” since he was the first to point out this gain [5 and 6]. This is the only reason

for building such an instrument and can be a powerful reason for weak sources.

In the case where the noise from the detector is due to signal photons (as for the photomultiplier tubes in the visible) then  $\xi$  is proportional to the square root of the incident radiation and the same signal-to-noise is obtained from the interferometer and above equivalent scanning instrument. The Michelson interferometer should not be used for general applications in this region.

A comparison of the usefulness of the Michelson interferometer with other interference techniques is presented by Jacquinet [9].

### 3. Construction and Design of a Michelson Interferometer

#### 3.1. General Description

It has been shown that a Michelson interferometer is useful in the infrared for obtaining optical spectra. Such an instrument has been built and will now be described. Figure 2 shows the optical and electronic layout. Several plane mirrors which only change the direction of the light beam, are omitted and focusing mirrors are shown as equivalent lenses for simplicity. The instrument was built to be used in the 3 to 4  $\mu$  region with a detector of lead sulfide or lead selenide. The maximum path difference available is about 80 cm and the aperture is

8 cm diam. The instrument was evacuated so that the index of refraction would be unity for all wavelengths. The source was imaged by spherical mirror  $F_1$  onto the entrance aperture. Off-axis parabolic mirror  $F_2$  collimates the light for the interferometer. The separating and compensating plates are mounted together for convenience. One arm of the interferometer has mirror  $M_1$  and the other arm has a cube corner, C.C., and mirror  $M_2$ . The cube corner slides on machined ways and has the property that light rays enter and leave it in parallel paths regardless of the cube corner's orientation. Its motion is controlled by a hydraulic system.

Off-axis parabolic mirror  $F_3$  focuses the fringes onto the exit aperture behind which sits the detector. The mirror  $F_3$ , the output aperture, and the detector, are at liquid nitrogen temperatures. The mirror  $M_3$  is half-silvered and is used for introducing into the interferometer light of wavelength 5461 Å from a mercury lamp for the purpose of alinement. A high intensity mercury lamp is used for the coarse adjustments, and a monoisotopic mercury lamp excited by a microtherm unit and cooled by blowing air, is used for the fine adjustments. Mirror  $M_3$  is slid to one side when the source is observed. An interference filter can be placed at the entrance aperture or at the exit aperture if a cold filter is desired. Radiation from the source is chopped at 640 c/s for discrimination against radiation emitted by the

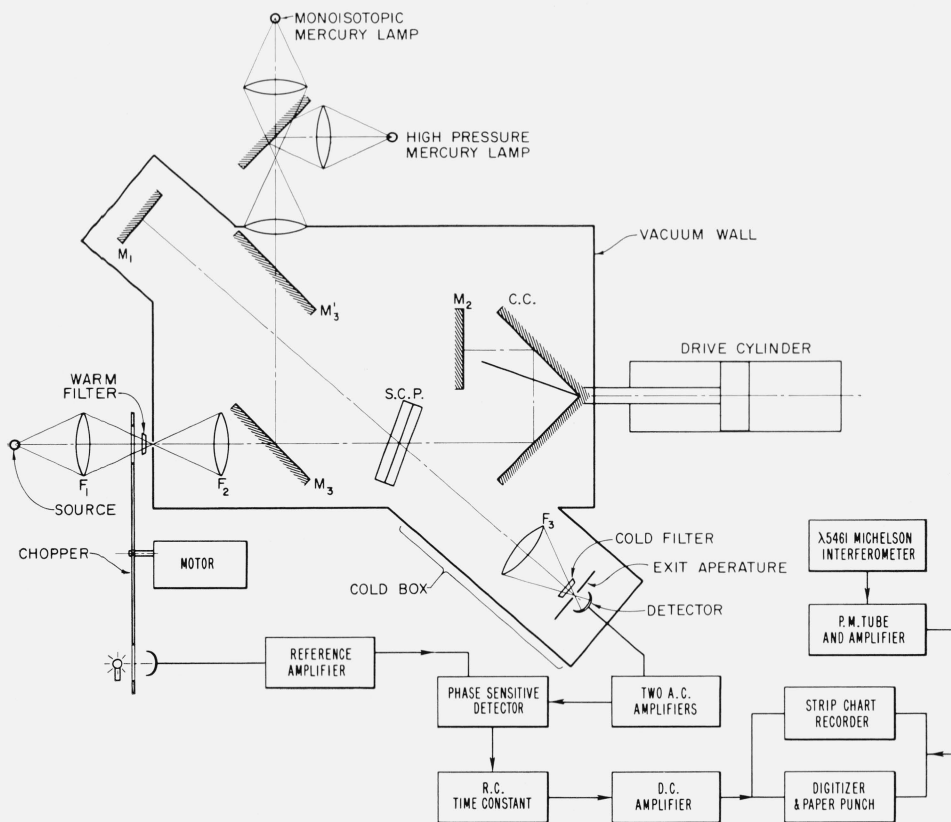


FIGURE 2. A schematic of the constructed Michelson interferometer.

optical components. The chopped interferogram is amplified and detected in a phase sensitive detector, the reference being derived from the chopper. A d-c amplifier supplies the correct signal voltages for the digitizer-paper punch unit and for the strip chart recorder. Care is taken that the only phase shifts in the electronics is in the R-C time constant after the phase sensitive detector.

Another Michelson interferometer is used to measure the path difference which has the cube corner as a common element with the main interferometer. This second interferometer is situated below the first interferometer. The 5461 Å line from the previously mentioned monoisotopic mercury lamp is used. Thus, this becomes a reference wavenumber or frequency. The fringes are detected by a photo-multiplier and are used to tell the digitizer when to take a reading. These reference fringes are also recorded on the strip chart recorder. A similar technique was first used by Connes and Gush [10] and is now employed by many people, e.g., Gebbie, Habell, and Middleton [11]. Some of the more interesting design details will now be pointed out.

### 3.2. Cube Corner

The design employing one cube corner in a Michelson interferometer was first suggested by Murty [12]. The design of using one cube corner, instead of two, is superior, as pointed out by Murty, due to the elimination of large lateral shifts of the fringes when the cube corner moves. The small fringe shifts present when one solid cube corner is used, are eliminated with a front surface cube corner. The tolerances required on the cube corner angles were calculated assuming that the misalignment of the wave front upon reflection from the cube corner should be less than or equal to  $\lambda/8$ . The result is that

$$\frac{\Phi\Delta}{\lambda} \leq 10^{-5} \quad (12)$$

where  $\lambda$  is in microns,  $\Delta$  is the maximum excursion in centimeters of the bumps on the slide or ways, and  $\Phi$  is the maximum error in radians of the cube corner angles. This formula applies to a cube corner 5 in. to 10 in. on one side. If  $\Delta = 10^{-2}$  cm,  $\Phi = \frac{10^{-3}}{3}$  radians, and  $\lambda = \frac{1}{2}\mu$ ,  $\Delta\Phi/\lambda = 10^{-5}$ . Therefore, the tolerance required on the  $90^\circ$  angles of the cube corner is less than 1 min of arc. The cube corner consists of three front surface mirrors glued together at angles of  $90^\circ$  to a tolerance of 1 sec of arc. Thus, almost any kind of machined ways can be used. Roller bearings sliding on stock steel rods were employed. The steel ways were situated in a plane containing the cube corner apex to minimize the rolling motion of the cube corner when it moves. The optical polish of the cube corner mirrors is limited by warpage of the plates when glued. It is suggested that optically contacting the surfaces should be superior, although more expensive. This technique was successfully used [13] for making a hollow cube of fused silica.

### 3.3. Cube Corner Drive System

The function of the hydraulic drive is to provide a smooth motion of the apex of the cube corner in one direction at a velocity of about  $2 \times 10^{-5}$  cm/sec. Both the long and short term stability of the drive are important as it is necessary to have the phase shifts for one wave number constant during a scan. The phase shifts in an electronic filter are, of course, a function of frequency. In general, a nut and screw gives a good long term stability but a poorer short term stability, while a hydraulic system is capable of a good short and long term stability. Figure 3 shows a schematic of the hydraulic system and is similar to one employed by Ameer and Benesch [14]. The 500 lb weight supplies a constant pressure of 1000 lb/in.<sup>2</sup> to the system. In the drive cylinder, there is more force pushing in the forward direction than in the opposite direction, hence the cube corner moves. The rate at which it moves is determined by the dimensions of the hypodermic tubing placed in the hydraulic circuit. Using Poiseuille's law of flow of liquid through a tube, it can be shown that the velocity of the cube corner is

$$V = \frac{\pi r^4 P A_2 - F}{8\eta l (A_1)^2} \quad (13)$$

where  $\eta$  is the viscosity of the fluid,  $r$  and  $l$  are the radius and length, respectively, of the hypodermic tubing.  $P$  is the pressure (1000 lb/in.<sup>2</sup>).  $A_1$  and  $A_2$  are the area of the drive cylinder piston and of the rod, respectively.  $F$  is the net force resulting from friction on the cube corner ways and in the drive cylinder rod seals. This frictional force will oscillate between the static and kinetic case due to the slow motion. In (13) only  $\eta$  and  $F$  can vary; the other quantities are rigidly fixed. Hence, upon

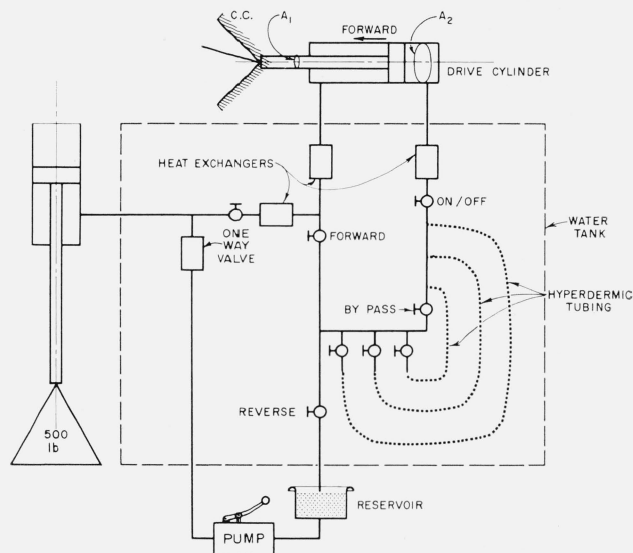


FIGURE 3. A schematic of the hydraulic drive system. The cube corner, c.c., can move in the forward or reverse directions.

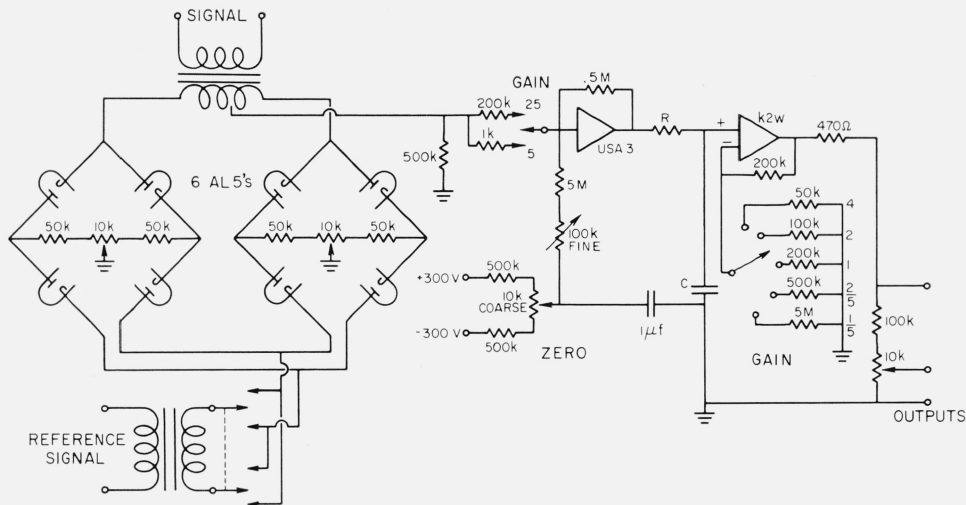


FIGURE 5. A schematic of the phase sensitive detector and d-c amplifier.

of 32 to 64  $\mu$  in. One O-ring should be used only once or twice and the flanges and O-ring should be degreased with chloroethene.

### 3.6. Electronics

The chopped interferogram is amplified and detected by the conventional a-c amplifier and phase sensitive detector method, commonly called a lock-in amplifier. Two a-c amplifiers are used, the first being a low level preamplifier which is mounted on the interferometer itself for shock mounting and elimination of pickup in long cables. The available gain is  $10^3$  to  $10^5$ . The signal and reference to the phase sensitive detectors are fed from cathode followers. Figure 5 shows the circuit of the phase sensitive detector, time constant, and d-c amplifier. The d-c amplifier employs operational amplifiers. A chopper stabilized amplifier supplies the required stability and a differential input operational amplifier supplies a high input impedance to the time constant. The signal required for the digitizer is about 0 to  $-10$  V. The photomultiplier and amplifier circuit for detecting the green fringes is similar to a design by Hunten [17]. This signal is used to order the digitizer to read and is also displayed on the strip chart recorder.

### 4. Performance

Figure 6 shows an interferogram obtained with a globar as source, a cold broadband filter, and a lead selenide detector. The globar was operated at a very low level (3 V across the 1.6  $\Omega$  globar) and the filter was a narrow band filter at 3.63  $\mu$  which suffered a permanent deterioration when cooled to liquid nitrogen temperatures. The resultant incident spectra consisted of two broadbands, one at 4  $\mu$  and the other at 6  $\mu$ , with bandwidths of 1.5  $\mu$  and 0.8  $\mu$ , respectively. The interferometer has a good response to the 4  $\mu$  band, but very little response to the

6  $\mu$  band, due to the separating plate. The reference mercury fringes are also shown and had a frequency of about 2 c/s. A time constant of 0.03 sec was used for the interferogram so that electronic phase shifts were not present. The interferogram demonstrates the following:

- (1) The instrument has excellent mechanical stability from interfering vibrations.
- (2) The stability of the cube corner drive is good.
- (3) The problem of phase shifts does not appear to be serious as the interferogram is symmetrical about a narrow zero order fringe. As the incident spectra had a large band width of 1.5  $\mu$ , any serious phase shifts would certainly have shown up.

The first two properties were forcibly demonstrated by observing on an oscilloscope the Lissajous figure made from an audio oscillator and the mercury

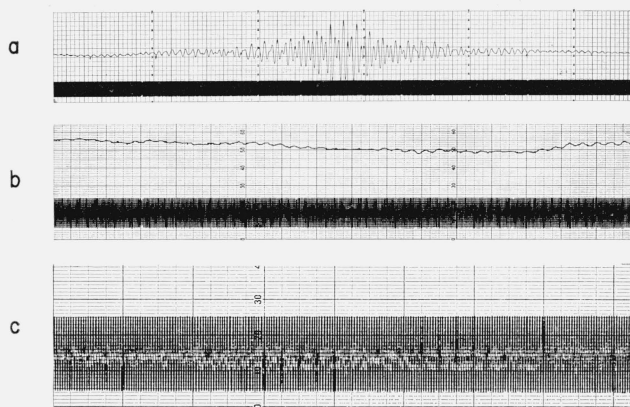


FIGURE 6. The interferogram obtained with the interferometer from a spectral band at 4  $\mu$  with a bandwidth of about 1.5  $\mu$ .

- a. Shows the interferogram around the position where the path difference is zero. It can be seen that the interferogram is symmetrical about the zero order fringe.
- b. Shows a portion of the interferogram at about 1 mm path difference.
- c. Shows a portion of the mercury reference fringes. The scale on figures b and c are expanded by a factor of 2 and 4, respectively, over figure a.

differentiation (13) becomes

$$-\frac{dV}{V} = \frac{d\eta}{\eta} + \frac{dF}{PA_2 - F} \quad (14)$$

Equation (14) shows that if the percentage change of the cube corner velocity is to be a minimum two conditions should be met. They are: (a)  $F \ll PA_2$  and (b)  $\frac{d\eta}{\eta}$  be a minimum. Now  $PA_2$  is 750 lb and  $F$  is one or two orders of magnitude less. This is the main reason for using a high pressure in the system. The frictional forces and thereby  $dF$  can also be reduced if air bearings are used; then  $P$  can be lower, resulting in an elegant and simple hydraulic system. Such a system has been built by Stroke [15 and 16], but would be difficult to incorporate in the Michelson interferometer in a vacuum. A hydraulic fluid was used which has a viscosity of about 50 cP at 70 °F and  $\frac{d\eta}{dt} \frac{1}{\eta}$  of about  $0.04/^\circ\text{F}$ . Thus, for the velocity of the cube corner to be constant to 4 percent, the oil should have a constant temperature to 1 °F. This is accomplished by placing the components of the system in a water bath and allowing oil which flows into these components to first pass through a heat exchanger which consists of a coil of tubing in the water bath. The large heat capacity of the water is sufficient to keep the temperature of the oil to better than 1 °F over the time of one scan; if a silicon oil was used,  $\frac{d\eta}{dt} \frac{1}{\eta}$  would be about  $0.01/^\circ\text{F}$ .

### 3.4. Mounting of the Optical Components

The interferometer is supported on small rubber inner tubes inflated to about 4 or 5 lb/in<sup>2</sup>. The mass of the instrument was intentionally made large for further stability from vibrations. The weight of the instrument is about 1000 lb. Each individual optical component is mounted by a type of ball joint and three adjusting screws, one of which is spring-loaded. The ball of the ball joint is a nut, which is tightened on a screw for mechanical stability. This type of adjustment constitutes the coarse adjustment and is illustrated in figure 4.

The fine adjustment of the parallelism of the interferometer plates (for the infrared and visible fringes) is made by tilting mirror  $M_1$ . This mirror has a coarse adjustment on its base plate and the mirror itself is supported on a shaft with a groove cut in it. Two springs placed 90° from each other relative to the center of the mirror are pulled to bend the shaft at its groove. A d-c motor turns a screw which pulls the springs. The mirrors  $M_1$  and  $M_2$  are flat to  $\lambda/20$  in the visible. The separating and compensating plates are made of calcium fluoride with dielectric coatings on the separating plate. They are used at an incidence angle of 20° to conserve their size. Their polish is to  $\lambda/3$  in the visible, their thicknesses are to 0.0005 in. or better, and the parallelism of the plates is to 3 sec of arc.

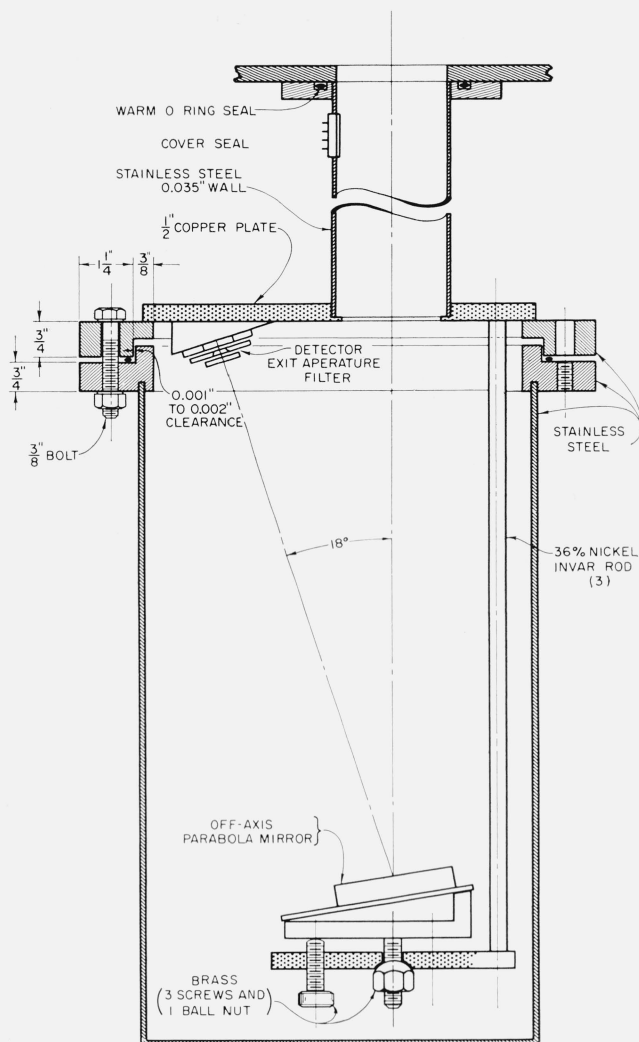


FIGURE 4. A schematic of the "cold box."

### 3.5. Cold Box

It was decided to use a lead selenide or lead sulfide cell cooled to liquid nitrogen temperatures as a detector. It was then simple to cool the exit aperture, interference filter, and the focusing mirror  $F_3$  of figure 2. Figure 4 shows the design. Liquid nitrogen covers the 1/2 in. copper plate which cools the attached detector, exit aperture, and filter. The off-axis parabolic mirror  $F_3$  of figure 2, is cooled mainly by radiation. The position of this mirror is kept fixed with respect to the detector as the contraction of the brass mounting and invar support rods are equal. Any tilting of the cold box is prevented by metal-to-metal contact at the warm O-ring seal. The cold O-ring seal employs a 1/8 in. O-ring with an i.d. about 3/4 in. undersize. It is of 60 or 70 durometer and is compressed to 1/5 of its thickness by 3,000 to 4,000 lb/in. compression supplied by 3/8 in. bolts spaced every 2 in. The O-ring surfaces should allow for the resulting flow of the O-ring and have a finish

fringe signal at about 20 c/s. There was very little motion of this figure over, say, a minute. However, there was a slow drift in the fringe signal frequency which amounted to about 5 percent in 5 min and 10 percent in 30 min. If this drift is serious, it may be possible to reduce it by simply continued operation of the hydraulic system, as there may still be some air in the system. A controlling mechanism could also be built to lock the signal frequency to some reference.

## 5. Conclusion

A Michelson interferometer with excellent mechanical stability and with an unusual drive system has been built and tested. Apparently, the hydraulic system gives a superior drive to the drive obtained from an expensive screw and nut with the exception of the long term stability.

Interferograms can now be obtained and recorded. The problems of calculating the spectra have not been completed, but involves solving the problem of obtaining a working relationship between the interferometer and computer, and possibly of improving the long term stability of the drive system.

---

This work was performed at the National Bureau of Standards under the supervision of David M. Gates for the USAF, Contract No. PRO 63-507.

The author would like to acknowledge the excellent machine work of P. F. Biddle and J. H. McCarron. Acknowledgements are due to R. H. Kropschot and D. H. Weitzel for advice on the cryogenic design of the cold box, and K. F. Nefflon for suggestions on some aspects of the interferometer design.

(Paper 69C1-179)

## 6. References

- [1] Michelson, A. (1891), Visibility of interference-fringes in the focus of a telescope, *Phil. Mag.* **31**, 256.
- [2] Michelson, A. (1892), On the application of interference methods to spectroscopic measurements II, *Phil. Mag.* **34**, 280.
- [3] Rayleigh, Lord (1892), On the interference bands of approximately homogeneous light; in a letter to Prof. A. Michelson, *Phil. Mag.* **34**, 407.
- [4] Rubens, H., and R. W. Wood (1911), Focal isolation of long heatwaves, *Phil. Mag.* **21**, 249.
- [5] Fellgett, P. (1951), The theory of infra-red sensitivities and its application to investigations of stellar radiation in the near infra-red, Thesis (Cambridge University).
- [6] Fellgett, P. (1958), A propos de la théorie du spectromètre interférentiel multiplex, *J. Phys. Radium* **19**, 237.
- [7] Jacquinet, P. (1958), Caractères communs aux nouvelles méthodes de spectroscopie interférentielle; facteur de mérite, *J. Phys. Radium* **19**, 223.
- [8] Connes, J. (1961), Recherches sur la spectroscopie par transformation de Fourier, *Rev. d'Optique* **40**, 45-78, 116-140, 171-190, 231-265.
- [9] Jacquinet, P. (1960), New developments in interference spectroscopy, *Rept. Progr. Phys.* **23**, 267.
- [10] Connes, J., and H. P. Gush (1959), Spectroscopie du ciel nocturne dans l'infrarouge par transformation de Fourier; *J. Phys. Radium* **20**, 915.
- [11] Gebbie, H. A., K. J. Hubell, and S. P. Middleton (1961), Michelson interferometers for spectrophotometry in the near infra-red region, *Optical Instruments Conference London* (1961).
- [12] Murty, M. V. R. K. (1960), Modification of Michelson interferometer using only one cube-corner prism, *J. Opt. Soc. Am.* **50**, 83.
- [13] Cook, A. H. (1961), Precise measurements of the density of mercury at 20° C, *Phil. Trans. Roy. Soc. London (A)* **254**, 125.
- [14] Ameer, G. A. and W. M. Benesch (1961), Interferometrically controlled hydraulic wavelength drive, *J. Opt. Soc. Am.* **51**, 303.
- [15] Stroke, G. W. (1958), Systems interférentiels a miroirs en mouvement continu et detection photo électrique, *J. Phys. Radium* **19**, 415.
- [16] Stroke, G. W. (1963), Interferometric method of velocity of light measurement, *Appl. Opt.* **5**, 481.
- [17] Hunten, D. M. (1953), A rapid-scanning auroral spectrometer, *Can. J. Phys.* **31**, 681.